ACADEMIC PRESS

Available online at www.sciencedirect.com

SCIENCE DIRECT®

Journal of Sound and Vibration 268 (2003) 917–931

JOURNAL OF SOUND AND VIBRATION

www.elsevier.com/locate/jsvi

The application of Duffing oscillator in characteristic signal detection of early fault

N.Q. Hu*, X.S. Wen

Research Institute of Mechatronics Engineering, College of Mechatronics Engineering and Automation , National University of Defense Technology, Changsha 410073, People's Republic of China

Received 16 January 2002; accepted 10 December 2002

Abstract

This paper presents a study of application of Duffing oscillator for extracting the features of early mechanical failure signal. By analysis of global solutions and bifurcation set of Duffing equation, we conclude that the bifurcation threshold, which corresponds to the maximum orbit outside the homoclinic orbit of Duffing equation, can be used to detect weak signal, such as the characteristic signal of early machinery fault. Therefore, the Duffing oscillator is suitable to be a model for weak signal detection, although some relative aspects for practical uses should be considered carefully. In this paper, the strategies for testing whether the weak signal is exists and how to estimate its amplitude are discussed in detail. Moreover, an example is presented here to demonstrate the utility of this method by analyzing the early rub-impact signal appearing in a rotor. The results show that the method is effective for early detection of fault described by specific periodic-motion components such as rub-impact fault of rotor in aeroengine.

1. Introduction

Biologists find that the vibration of a human eardrum is non-symmetrical, and the potential of eardrum vibration can be described by the following equation:

$$U = \tfrac{1}{2}\kappa x^2 + \tfrac{1}{3}\lambda x^3. \tag{1}$$

If the effective mass of eardrum be normalized as unity, then the motion equation of eardrum can be simplified as

$$\ddot{x} + \kappa x + \lambda x^2 = 0. \tag{2}$$

*Corresponding author.
E-mail address: hnq_5744@163.com (N.Q. Hu).

0022-460X/03/$ - see front matter
doi:10.1016/S0022-460X(03)00002-6

The sound signal (including basis and higher-term harmonics) can be written as

$$F = \sum_{i=1} F_i \cos(\omega_i t + \theta_i). \tag{3}$$

With the sound signal entering the auricle, we obtain the motion- equation of eardrum:

$$\ddot{x} + \kappa x + \lambda x^2 = \sum_{i=1} F_i \cos(\omega_i t + \theta_i). \tag{4}$$

It is well-known that human ears have the ability to identify weak sound with high resolution. If the model of a human eardrum described by Eq. (4) is appropriate, we can imagine that the ability of human ears is associated with parameters κ, λ, F_i and so on. Thus, we may use Eq. (4), the nonlinear oscillator or Duffing oscillator, as a model, to detect weak signal by means of adjusting its parameters. Now, we describe the basic idea as follows.

If the signal needed for detection is the perturbation of external periodic force of chaotic oscillator (Duffing equation) [1–3], the noise component in the signal cannot induce the state transition of the oscillator even if it is very strong. Furthermore, the weak fault-signal component, with specific characteristics like periodic signal, can make the oscillator produce phase shift, under these conditions, we can identify the fault signal with the specific feature by calculating the states of the oscillator.

Some of the literature discusses how to use the Duffing equation to detect weak signal and diagnose incipient fault, but the solutions of Duffing equation, which play an important role in practical uses, have not been discussed in detail [1–4,8]. Therefore, in this paper, we will discuss related problems about the solutions of Duffing equation and implementing model for detecting the weak signal based on the characteristics of the solutions.

2. Global solutions and bifurcations of duffing equation

Consider the simplest Duffing equation [5–7]:

$$\ddot{x} - x + x^3 = 0. \tag{5}$$

By introducing the signals of the weak dissipation (aerodynamic damping) and periodic force, we obtain

$$\ddot{x} - x + x^3 = \varepsilon(\gamma \cos \omega t - \delta \dot{x}), \tag{6}$$

Eq. (6) can be written as a set of state equation:

$$\begin{aligned} \dot{x} &= y, \\ \dot{y} &= x - x^3 + \varepsilon(\gamma \cos \omega t - \delta y), \end{aligned} \tag{7}$$

where the force amplitude γ, frequency ω, and the damping δ are variable parameters and ε is a small scaling parameter. Solving Eq. (7) for $\varepsilon = 0$, we obtain a center at $(x, y) = (\pm 1, 0)$ and a hyperbolic saddle at $(0, 0)$. The level set of Eq. (7) can be written as

$$H(x, y) = \frac{y^2}{2} - \frac{x^2}{2} + \frac{x^4}{4} = 0, \tag{8}$$

which includes two homoclinic orbits, Γ_+^0, Γ_-^0 and a point $p_0 = (0, 0)$ as shown in Fig. 1.

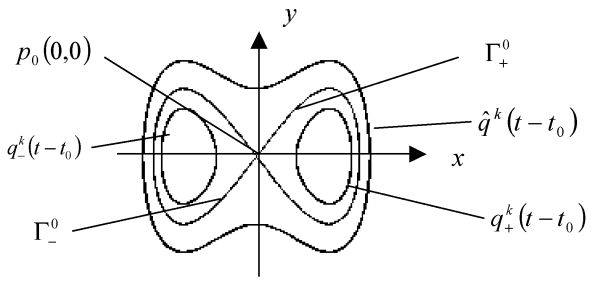

Fig. 1. Unperturbed resonant level curves.

The unperturbed homoclinic orbits are given by

$$q_+^0(t-t_0) = \left[\sqrt{2}\,\mathrm{sech}(t-t_0), -\sqrt{2}\,\mathrm{sech}(t-t_0)\tanh(t-t_0)\right],$$
$$q_-^0 = -q_+^0. \tag{9}$$

Within each of the loops $\Gamma_\pm^0$, there is a family of periodic orbits with one-parameter k, which may be written as

$$q_+^k(t-t_0) = \left[\sqrt{\frac{2}{2-k^2}}\,\mathrm{d}n\left(\frac{t-t_0}{\sqrt{2-k^2}},k\right), \frac{-\sqrt{2}k^2}{2-k^2}\,sn\left(\frac{t-t_0}{\sqrt{2-k^2}},k\right)\,cn\left(\frac{t-t_0}{\sqrt{2-k^2}},k\right)\right],$$
$$q_-^k(t-t_0) = -q_+^k(t-t_0), \tag{10}$$

where sn, cn and dn are the Jacobi elliptic functions and k is the elliptic modulus. As $k\to 1, q_\pm^k \to q_\pm^0 \cup \{0,0\}$, as $k\to 0, q_\pm^k \to (\pm 1, 0)$. Selecting initial conditions at $t = t_0$, we have

$$q_\pm^0(0) = \left(\pm\sqrt{2}, 0\right), \quad q_\pm^k(0) = \left[\pm\sqrt{\frac{2}{2-k^2}}, 0\right]. \tag{11}$$

The orbits lying outside $\Gamma_+^0 \cup \{(0,0)\} \cup \Gamma_-^0$ are given by

$$\hat{q}^k(t-t_0) = \left[\sqrt{\frac{2k^2}{2k^2-1}}\,cn\left(\frac{t-t_0}{\sqrt{2k^2-1}},k\right), -\frac{\sqrt{2}k}{2k^2-1}\,sn\left(\frac{t-t_0}{\sqrt{2k^2-1}},k\right)dn\left(\frac{t-t_0}{\sqrt{2k^2-1}},k\right)\right], \tag{12}$$

where $k \in \left(1/\sqrt{2}, 1\right)$, and $\hat{q}^k \to q_+^0 \cup \{(0,0)\} \cup q_-^0$ as $k\to 1$ and $\hat{q}^k$ becomes unbounded as $k \to 1/\sqrt{2}$.

With reference to Melnikov function, we can obtain the following bifurcation threshold $R^0(\omega)$ for q_+^0 (or q_-^0):

$$R^0(\omega) = \frac{\gamma}{\delta} = \frac{4\cosh(\pi\omega/2)}{3\sqrt{2}\pi\omega}. \tag{13}$$

In Eq. (13), if $\gamma/\delta > R^0(\omega)$, the stable manifold intersects unstable manifold for ε is small enough and if $\gamma/\delta < R^0(\omega)$, the intersection of stable manifold and unstable manifold is empty.

Consider the resonance orbits $q_+^k(t-t_0)$ within Γ_+^0, the bifurcation threshold $R^m(\omega)$ is

$$R^m(\omega) = \frac{\gamma}{\delta} = \frac{J_1(m,1)}{J_2(m,1,\omega)}, \tag{14}$$

where

$$J_1(m,n)=\frac{2}{3}\frac{\left[2-k^2(m,n)\right]2E[k(m,n)]-4k'^2(m,n)K[k(m,n)]}{[2-k^2(m,n)]^{3/2}}$$

and

$$J_2(m,n,\omega)=\begin{cases}0, & n\neq 1\\ \sqrt{2}\pi\omega\ \mathrm{sech}\left(\dfrac{\pi m K'[k(m,1)]}{K[k(m,1)]}\right), & n=1\end{cases}$$

Here $E(k)$ is the complete elliptic integral of the second kind and k' is the complementary elliptic modulus $k'^2=1-k^2$.

From Eq. (14), if $\gamma/\delta > R^m(\omega)$ there are a pair of m order sub-harmonics (period $2\pi m/\omega$) which appear on a bifurcation curve tangent to the curve $\gamma=R^m(\omega)\delta$ at the point $\gamma=\delta=0$ [5].

By a similar procedure, we can obtain the orbits lying outside $\Gamma_+^0\cup\{(0,0)\}\cup\Gamma_-^0$,

$$\hat{R}^m(\omega)^{def}=\frac{\gamma}{\delta}=\frac{\hat{J}_1(m,1)\delta}{\hat{J}_2(m,1,\omega)} \tag{15}$$

with

$$\hat{J}_1(m,n)=\frac{2\left[2k^2(m,n)-1\right]4E(k(m,n))+4k'^2(m,n)K[k(m,n)]}{3[2k^2(m,n)-1]^{3/2}}$$

and

$$\hat{J}_2(m,n,\omega)=\begin{cases}0, & n\neq 1,\ \ m\ \text{even},\\ 2\sqrt{2}\pi\omega\ \mathrm{sech}\left(\dfrac{m\pi K'(m,1)}{2K(k(m,1))}\right), & n=1,\ \ m\ \text{odd}.\end{cases}$$

Here $k(m,n)$ is the unique solution of the following resonance equation:

$$\hat{T}_k=4K(k)\sqrt{2k^2-1}=\frac{2\pi m}{\omega n}. \tag{16}$$

In addition, according to the transform formula of dual active-angle variables and related theory, we can analyze the higher order terms and the stability of the global solutions of Duffing equation. Then we can find the attractor of sub-harmonics, that is

$$\Delta I(m)\sim\sqrt{\left(\varepsilon\frac{m^3}{4\omega^3}\right)}\exp(-\pi m/\omega). \tag{17}$$

We can see that the attractor will shrink rapidly in size as m is increased. This means that the bands of resonance will become more and more narrow. Only the bands of the lower order sub-harmonics have sufficient width [5,6].

By the above analysis, we have obtained three types of bifurcation thresholds, $R^0(\omega), R^m(\omega), \hat{R}^m(\omega)$ of Duffing equation.

As an example of $\omega=1$, Fig. 2 shows how the bifurcation thresholds of homoclinic, sub-harmonic inside and outside homoclinic orbits vary with $\varepsilon\delta$ and $\varepsilon\gamma$.

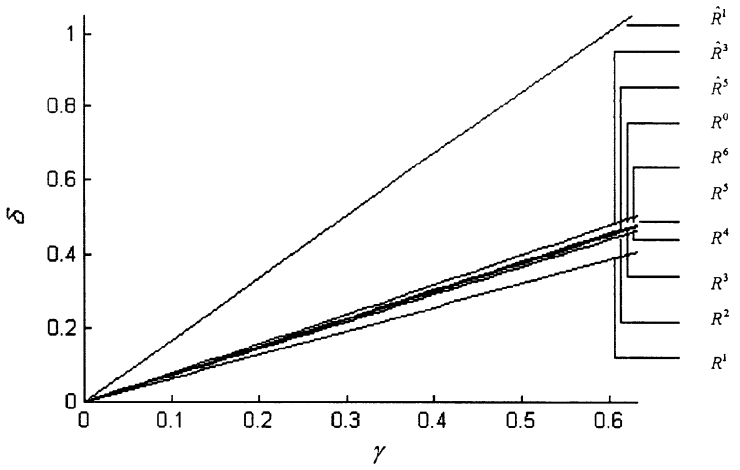

Fig. 2. Bifurcation thresholds of R^0, R^m, R^m vary with $\varepsilon\delta$ and $\varepsilon\gamma$.

In Fig. 2, $\hat{R}^1$ is quite different from the others. This phenomenon can be seen as useful information for detection of weak signal. In the meantime, from Eq. (17), we see that attractors shrink rapidly in size as m increases. That is, the width of resonance band approaches zero ($\Delta I \to 0$) when m approaches infinity ($m \to \infty$). The resonance band of sub-harmonic is sufficiently wide only in the case of $m = 1$. Thus, we mainly focus on the property of shift phase of the outside orbit as $m = 1$, and use the property to detect weak signal.

Selecting the outer orbit in case of $m = 1$ to be the detected orbit has many advantages [2]. From Fig. 2, under the condition of diverse δ, the bifurcation value of $\hat{R}^1$ is obviously greater than those of others, and the set of orbits converts into periodic sub-harmonic motion which is steadily in sub-harmonic orbit of $m = 1$ when $\gamma/\delta > \hat{R}^1$. The ultimate motion of this transition is obvious. From Eq. (17), the width of resonance band of sub-harmonic, in case of $m = 1$, is the greatest and it can guarantee that the points in phase domain are steadily within resonance band even if γ and δ are very great. Theoretically, γ is linear to δ when δ varies over a rather large range. Because the parameters, γ and δ, can be endowed with quite big values, it is easy to guarantee that the form of ultimate motion of the orbits is always in the orbit of the global chaotic state when γ/δ is quite less than $\hat{R}^1$, no matter where the initial point of attractor is. In the meantime, when γ/δ is greater than R^m ($m = 1, 2, \ldots$) and $\hat{R}^m$ ($m = 3, 5, \ldots$), the trajectory in phase domain will be steady in these orbits. But because the resonance bands of these sub-harmonic orbits are so narrow that any γ and δ cannot make the set of solutions be steady in any orbit even if they are endowed with quite big values, this form of the ultimate motion reveals chaotic motion.

3. Detecting model and refinement of bifurcation value

3.1. Detecting model

According to the theoretical analysis mentioned in Section 2, the orbit, in case of $m = 1$, is the largest orbit which departs farthest away from homoclinic orbits among the set of solutions

outside homoclinic orbits of Duffing equation. Consider the case of $\omega = 1$, we rewrite the Duffing equation as

$$\ddot{x} + \delta\dot{x} - x + x^3 = \gamma \cos t. \tag{18}$$

By computation of the theoretical bifurcation value of Eq. (18), we know that the chaotic motion is transforming into periodic motion when $\hat{R}^1 = \gamma_c/\delta = 1.676889$. That is, if the amplitude of external exciting periodic force is $\gamma = \gamma_c = \delta\hat{R}^1$ or little less than this value, Eq. (18) will experience chaotic and periodic motion alternately as time goes on.

The detecting model is constructed as follows:

$$\ddot{x} + \delta\dot{x} - x + x^3 = \gamma_c \cos t + s(t), \tag{19}$$

where the first term of right side of Eq. (19) is the referenced signal and the second term is the signal to be detected. If the frequency of $s(t)$ is the same as that of the referenced signal, the system described by Eq. (19) will cause a phase shift in spite of the weak amplitude. This means the system will convert the chaotic motion into a large periodic motion. When the frequency of weak signal $s(t)$ is different from that of referenced signal, the system will not induce phase shift. This property of bifurcation can be used as a means for detecting weak signal [8].

3.2. Discretization influence for bifurcation value

Considering the bifurcation of the set of solutions of Eq. (19), we know theoretically that the condition of converting chaos into periodic motion is $\gamma_c/\delta = \hat{R}^1 = 1.676889$, where γ_c is the critical value of γ as δ is fixed. In fact, the signals we have dealt with in laboratory are often in the form of time series. However, the bifurcation value discussed so far is in the continuous form since it is derived from calculation. We do not apply the bifurcation threshold to signal detection. In practice, the bifurcation threshold determined by numerical computation is slightly less than the theoretical value.

Discretizing Eq. (18) and solving it by using Runge–Kutta method, we can obtain a discrete equation. The similarity between discrete equation and original equation is governed by the integral iteration step h. Different h results in $\hat{R}^1$ with slight difference. In the following, we shall determine the changing trend of $\hat{R}^1$ by numerical analysis. First, we fix h and δ. Then, determine the critical value γ_c of phase shift by numerical computation. Some of the results are shown in Tables 1 and 2. (The initial time is 0.0 s, initial point is $(x, \dot{x}) = (1.0, 1.0)'$, the length of time series is 20 000.)

Further numerical analysis shows that the ultimate form of motion determined by Eq. (19) is always in sub-harmonic orbit in case of $m = 1$ when $\gamma/\delta > \hat{R}^1$, no matter how big γ is, the trajectory is of slight distortion.

Table 1
Small change of $\hat{R}^1$ when $h = 0.01$

δ	0.3	0.4	0.5	0.6	0.7	0.8
γ_c	0.5177	0.6725	0.8276	0.9816	1.1372	1.28
$\hat{R}^1$	1.7257	1.6812	1.6551	1.636	1.6245	1.60

Table 2
Small change of $\hat{R}^1$ when $h = 0.005$

δ	0.3	0.4	0.5	0.6	0.7	0.8
γ_c	0.5177	06724	0.8275	0.9786	1.2614	1.3696
$\hat{R}^1$	1.7257	1.6811	1.655	1.631	1.802	1.712

3.3. The evolution of bifurcation from chaos to periodic motion

For convenience and without loss of generalization, we select parameters of $h = 0.005$ and $\delta = 0.5$ for analysis of the solutions (orbits). In the cases of $R = 1.60$, 1.654, 1.655, 1.656, we obtain the time histories and phase portraits corresponding to different R as shown in Fig. 3(a), (b), (c) and (d), respectively.

Fig. 3(a) is in the chaotic state. Fig. 3(b) and (c) are chaotic and periodic motions appearing alternately, that is, one can observe the intermittent chaotic phenomena. The width of chaotic contour becomes more and more narrow with increase in the value R. In Fig. 3(d), the orbit becomes completely a large orbit of periodic motion. Thus, in the case of $h = 0.005$, $\delta = 0.5$, and $\omega = 1$, $\gamma_c = 0.5 \times 1.655 = 0.8275$ is the bifurcation point of chaotic and periodic motions.

From the above figures, we can observe that when R changes from 1.60 to 1.655, the output of resonator is mixed with the chaotic and periodic motions, and the chaotic state is gradually replaced by the periodic motion as the value of R increases. The orbit becomes a large periodic motion at the point $R = 1.656$. Therefore, $\hat{R}^1 = 1.655$ is sensitive to weak signal. At the meantime, the amplitude of referenced signal is $\gamma_c = 0.5 \times 1.655 = 0.8275$. If the amplitude of the weak signal is not less than $A = 0.5 \times 0.001 = 0.0005$, and R is not less than 1.656, the resonator is a large periodic motion as shown in Fig. 3(d),

If quite a strong noise, such as a white noise without loss of generalization, is added to the weak signal, the results of Fig. 3(d) will not be so "ideal". There is a very short "chaotic contour" mixed with a large periodic response. It is not easy to judge phase shift by Fig. 3. Therefore, it is necessary to search for a reliable and fast method to determine phase shift quantitatively, so as to exert the potential function of chaotic resonator in detecting the weak signal. We discuss this in detail in another paper.

4. Further discussion of related problems

If γ is 0.8275 or slightly less than that in Eq. (19), chaotic and periodic motions will occur alternately in the ultimate state of the orbits. At the same time, the orbits are perturbed by external weak signal (for example, $s(t) = 0.0005 \cos t$), the frequency of which is the same as the referenced signal. We rewrite Eq. (19) as

$$\ddot{x} + \delta\dot{x} - x + x^3 = 0.8275 \cos t + s(t). \tag{20}$$

Now the ultimate state of motion is the same as that shown in Fig. 3(d), and the orbits have transited from chaos to periodic motion. Through this process, weak signal such as $0.0005 \cos t$ can be detected. But for practical uses, we must first solve a series of problems.

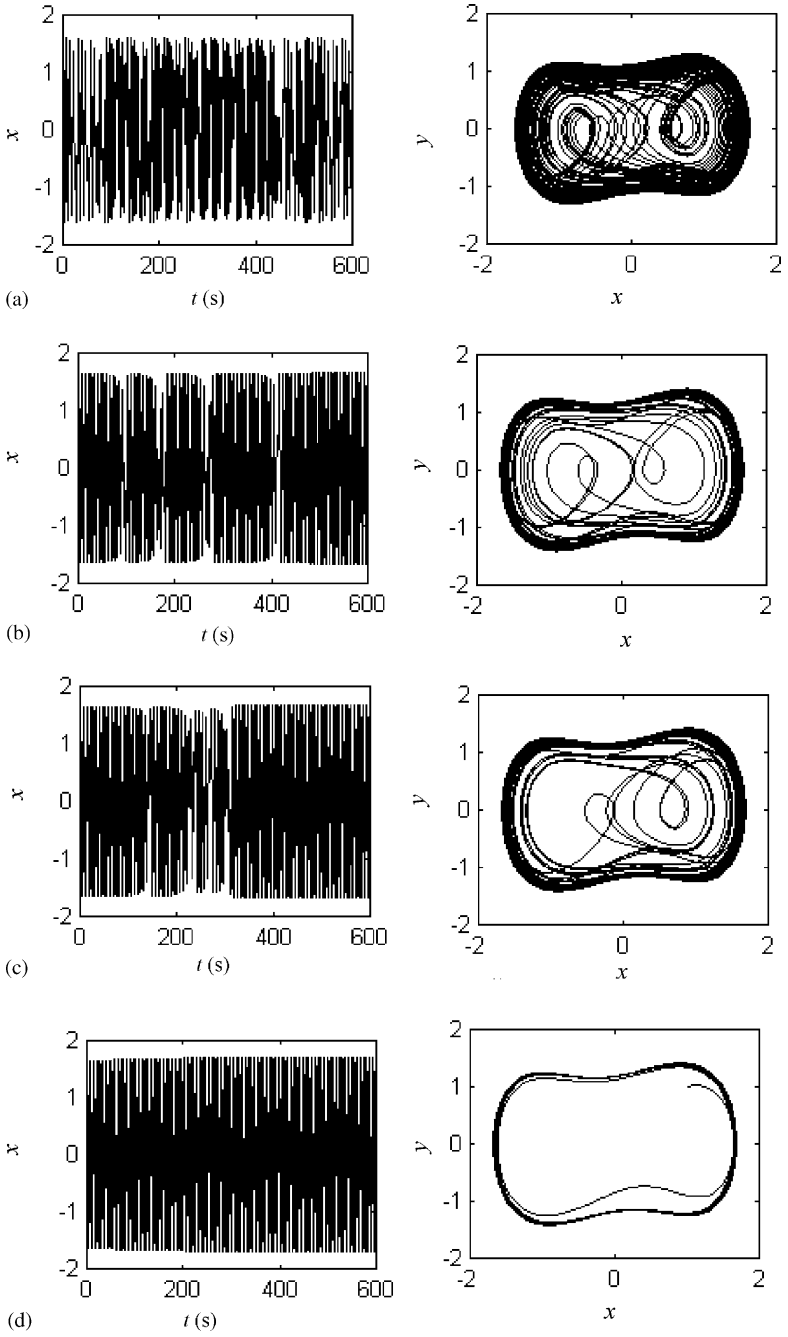

Fig. 3. Time histories and phase portraits of detected model outputs: (a) $h=0.005$, $\delta=0.5$, $R=1.60$; (b) $h=0.005$, $\delta=0.5$, $R=1.654$; (c) $h=0.005$, $\delta=0.5$, $R=1.655$; (d) $h=0.005$, $\delta=0.5$, $R=1.656$.

4.1. Influence of noise

If external exciting signal is pure noise $s(t) = \varepsilon(t)$, that is, the right side of Eq. (20) becomes $0.8275 \cos t + \varepsilon(t)$, can we use the orbits determined by Eq. (20) to reveal the orbit shift? Assuming the external noise is Gaussian, we consider the cases of $\varepsilon(t) \sim N(0, 1)$ and $\varepsilon(t) \sim N(0, 3.5^2)$, and the solutions of Eq. (20) are shown in Fig. 4(a) and (b). Obviously, we can see that there is no orbit shift in Fig. 4. The orbits are in chaotic state which means that the orbits can keep the state of motion steadily under the influence of the perturbation of noise.

4.2. Influence of to-be-detected signal added noise

If the external exciting signal is $s(t) = 0.0005 \cos t + \sigma\varepsilon(t)$, will the orbit shift occur or not? If so, what is the upper limit of σ? Furthermore, what is the threshold of the signal-and-noise ratio at which the weak signal can be detected? Assuming the exciting signal consists of the noise and weak signal with the identical frequency as that of the referenced signal, that is $s(t) = 0.0005 \cos t + 0.5\varepsilon(t)$, we solve Eq. (20) again and the result reveals that the phase of the orbits shift at the value of the mean square root $\sigma = 0.5$, and the weak signal $0.0005 \cos t$ can be detected reliably. By similar approaches, and letting $\sigma = 1.0, 0.6, 0.4$ for trial, we observe that when $\sigma > 0.5$, the weak signal is buried by noise thoroughly, and thus, it cannot be detected. Only if $\sigma \leqslant 0.5$, can the weak signal be identified reliably. Therefore, we can estimate the threshold of the signal-and-noise ratio of the weak signal should be greater than

$$SNR = 20 \log \frac{0.0005/\sqrt{2}}{0.5} = -63 \quad \text{(dB)}.$$

Otherwise, it is not detectable by the method mentioned above.

4.3. Influence of different frequency signal

If the frequency of external signal is different from that of referenced signal, for example, $s(t) = 0.005 \cos \omega t$, where $\omega = 0.5$, 2, 10, or 200, will the orbits shift from one state to another or not? For trial, letting $\omega = 0.5, 2.0, 10.0, 200.0$, we again solve Eq. (20), the results show that the orbits keep chaotic state and there is no evidences that the state of motion is shifted. In these cases, the frequencies ω of the external signals are always the integral multiple of that of the referenced signal since the frequency of referenced signal is selected as $\omega = 1$. In theory, it is

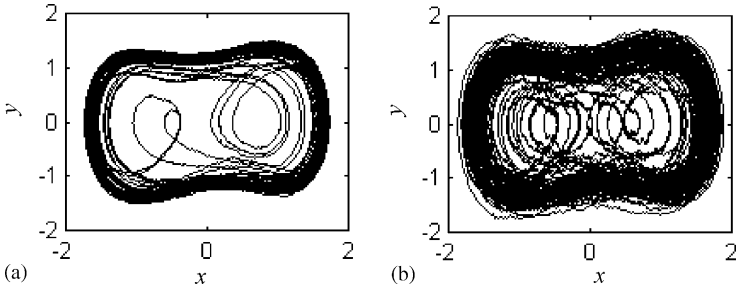

Fig. 4. The state of system after perturbation of noise: (a) the case of $\sigma = 1.0$; (b) the case of $\sigma = 3.5$.

possible that the state of motion will be shifted by the influence of these signals, but the premise of this phenomenon is that the amplitudes of these signals must be big enough. That is, if the amplitudes of external signals are sufficiently small, then the state of motion will not shift when the frequency of the external signal is integral times of that of the referenced signal.

4.4. Detecting result of signal with frequency-shift

If the frequency of the external signal is slightly different from that of the referenced signal, for example, $s(t) = 0.0005\cos[(1 \pm \Delta\omega)t]$, can the orbits be shifted or not? If so, what is the limit of $\Delta\omega$? Assume that the signal to be detected is $s(t) = 0.0005\cos[(1 \pm \Delta\omega)t]$, letting $\Delta\omega = 0.01$, 0.03, 0.05, 0.06, and 0.07, respectively, then the solutions of Eq. (20) show that orbits are shifting at the domain of $|\Delta\omega| \leqslant 0.05$.

4.5. Influence of initial phase

If there is a difference of initial phase between the external signal and the referenced signal, for example, $s(t) = 0.005\cos[t + \varphi_0]$, will the orbit transition occur?

Letting the referenced signal be $\gamma_c \cos t$, and the weak signal be $V\cos(t + \varphi_0)$, then we can write the total periodic exciting force as

$$\begin{aligned} A(t) &= \gamma_c \cos t + V\cos(t + \varphi_0) \\ &= (\gamma_c + V\cos\varphi_0)\cos t - V\sin\varphi_0 \sin t \\ &= \gamma(t)\cos(t + \phi(t)), \end{aligned} \tag{21}$$

where $\gamma(t) = \sqrt{\gamma_c^2 + 2\gamma_c V\cos\varphi_0 + V^2}$, $\phi(t) = \mathrm{arctg}(V\sin\varphi_0/(\gamma_c + V\cos\varphi_0))$.

It can be seen from Eq. (19) that the orbit shift is related to the difference of phase between the external signal and the referenced signal. When $\pi - \arccos(V/2\gamma_c) \leqslant \varphi_0 \leqslant \pi + \arccos(V/2\gamma_c)$, and $\gamma(t) \leqslant \gamma_c$, the orbit transition will not occur. This conclusion can be validated as follows:

Considering Eq. (20) again, if $h = 0.005$ and $s(t) = 0.005\cos(t + \varphi_0)$, we know that, by theoretical computation, the orbit shift will not occur when $\varphi_0 \in [1.5738, 4.7094]$. In practice, however, the range (about [1.9,4.6]) of the difference phase between the external and the referenced signals in which the orbit shift occurs is much more narrow than the theoretical result because of the effect of discretization. If the amplitude V of the weak signal is big enough, the range of the phase difference in which no orbit transition occurs becomes wider. In this case, we must consider the affect of the magnitude of the difference of phase. Some measures must be taken to make the phase of the external signal match that of the referenced signal.

4.6. Detecting method for signal with any frequency

So far we have mainly dealt with the signal with very low frequency ($\omega = 1$). If the frequency ω of weak signal is greater than one, how can we detect it?

In case of the weak signal with any frequency, the co-ordinates of Eq. (18) need to be transformed [2].

Considering Eq. (18), letting $t = \omega_0\tau$, we obtain

$$\begin{aligned} x(t) &= x(\omega_0\tau) = \bar{x}(\tau), \\ \frac{\mathrm{d}x(t)}{\mathrm{d}t} &= \frac{1}{\omega_0}\frac{\mathrm{d}x(\omega_0\tau)}{\mathrm{d}\tau} = \frac{1}{\omega_0}\frac{\mathrm{d}\bar{x}(\tau)}{\mathrm{d}\tau}, \\ \frac{\mathrm{d}^2x(t)}{\mathrm{d}t^2} &= \frac{1}{\omega_0^2}\frac{\mathrm{d}^2x(\omega_0\tau)}{\mathrm{d}\tau^2} = \frac{1}{\omega_0^2}\frac{\mathrm{d}^2\bar{x}(\tau)}{\mathrm{d}\tau^2}. \end{aligned} \tag{22}$$

Substituting Eq. (22) into (18), and omitting the upper score of variable $\bar{x}$, we get

$$\frac{1}{\omega_0^2}\frac{\mathrm{d}x^2}{\mathrm{d}\tau^2} + \frac{\delta}{\omega_0}\frac{\mathrm{d}x}{\mathrm{d}\tau} - x + x^3 = \gamma_c\cos(\omega_0\tau). \tag{23}$$

Adding the signal $a\cos((\omega_0 + \Delta\omega)\tau + \varphi)$ in the right side, we have

$$\begin{aligned} &\frac{1}{\omega_0^2}\frac{\mathrm{d}x^2}{\mathrm{d}\tau^2} + \frac{\delta}{\omega_0}\frac{\mathrm{d}x}{\mathrm{d}\tau} - x + x^3 \\ &\quad = \gamma_c\cos(\omega_0\tau) + a\cos((\omega_0 + \Delta\omega)\tau + \varphi) = A(\tau). \end{aligned} \tag{24}$$

Let $x = x, y = (1/\omega_0)(\mathrm{d}x/\mathrm{d}\tau)$, Eq. (24) can be written as a set of state equations:

$$\frac{\mathrm{d}x}{\mathrm{d}\tau} = \omega_0 y, \quad \frac{\mathrm{d}y}{\mathrm{d}\tau} = \omega_0(-\delta y + x - x^3 + A(\tau)). \tag{25}$$

Comparing Eq. (25) with Eq. (19), we see that $\dot{x}$ and $\dot{y}$ are multiplied by ω_0. Since Eq. (25) is obtained from Eq. (19) by linear transition, some of the properties of the state of motion, such as bifurcation value $\gamma/\delta = R^0(\omega), R^m(\omega), \hat{R}^m(\omega)$, do not change.

The results obtained by numerical computation for Eq. (25) demonstrate that $\hat{R}^1(\omega_0)$ increases slightly as ω_0 increases. The range of ω_0 in which the orbit of large-scale period does not distort is related to sampling step h when $\gamma/\delta > \hat{R}^1(\omega_0)$. The smaller the step h is, the wider the detected range of ω_0 becomes.

4.7. Determining amplitude for weak signal with any frequency

Having detected the existence of the weak signal, we shall focus mainly on how to determine the amplitude of the signal.

Under the circumstance of the periodic motion of the resonator, namely $\gamma > \gamma_c = \hat{R}^1(\omega)\delta$, the greater the amplitude γ of exciting signal is, the greater the amplitude A of response becomes. It is easy to understand, if $\omega h = Const$, then the amplitude A will vary with γ consistently. A series of results are shown in Fig. 5. When ω increases gradually from one unit, the amplitude A varies with γ gradually. According to results shown in Fig. 5, we see that the amplitude A is proportional to γ which changes from 0.84 to 0.94. Thus, we can fit a curve $A(\gamma)$ as follows:

$$A(\gamma) = 0.927995\gamma + 0.932917. \tag{26}$$

The procedure of determining the amplitude is described as follows:

According to the numerical solution of Eq. (25), we can obtain the amplitude A of a periodic response. Reading the corresponding γ in Fig. 5, or solving γ from Eq. (26), and subtracting γ_c from γ, then we obtain the amplitude of signal which is equal to $\gamma - \gamma_c$.

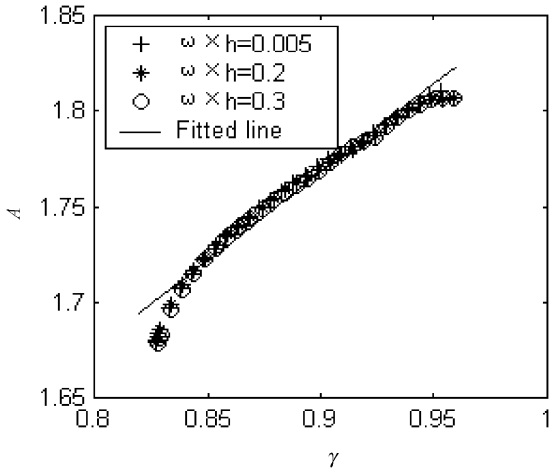

Fig. 5. Amplitude A varying with γ.

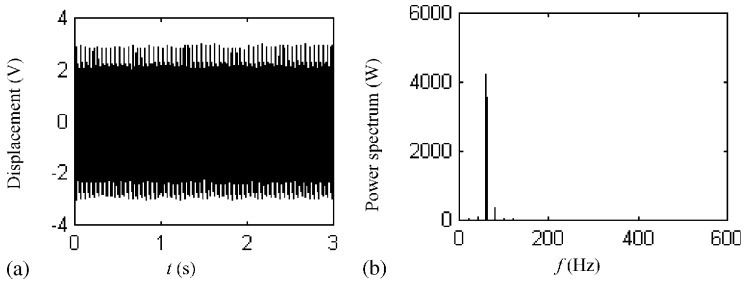

Fig. 6. Vibration displacement data $s1(n)$ of early rotor rub-impact: (a) waveform and (b) power spectrum.

So far, we have given detailed analysis of estimating amplitude and frequency of the weak signal via chaotic oscillator. In the following, we shall give an example of detecting the inceptive rub-impact signal of a rotor system.

5. An example of application

Refs. [9,10] had carried out a detailed experimental research on vibration characteristics of the sharp rub-impact of a rotor. The results show that, under some rotating speed, the responses of the weak signal, caused by the rotor rubbing against the stator at early stage, are sub-harmonic vibrations with a series of order which are the multiples of $1/n$ (generally $n = 3$). These results are of great significance to early diagnostics of the rub-impact of a rotor system. By means of the chaotic resonator method, under the circumstance of noise,we can detect the weak periodic signals with specific frequency which represent the symptom of early fault.

To demonstrate the effectiveness of the method of chaotic resonator in identifying the feature of early rub-impact fault, we collected 3000 points of radial vibration signals (denoted by $s1(n)$) from a rotor rub-impact rig with a sampling frequency 1000 Hz as shown in Fig. 6(a). We can see the spectrum lines of $1/3X$ (20 Hz), $2/3X$ (40 Hz), $4/3X$(80 Hz) standing out in the Fig. 6(b), where X denotes frequency of rotating speed which is equal to 60 Hz. However, by using the classical method, such a weak signal mixed with noise cannot be distinguished with naked eyes in spectrum graph.

In any case, the frequency of rotating speed is a multiple of $1/3X$ and the amplitude of the signal is very big. Supposing $s1(n)$ to be the perturbation signal of the rotor system, whether the signal $(1/3X)$ is mixed in $s1(n)$ or not, the chaotic oscillator may produce state transition and therefore we shall obtain a false result about the existence of $1/3X$ representing early rub-impact. For the purpose of detecting the inceptive rub-impact of the rotor, we need to detect $1/3X$, $2/3X$, $4/3X$ [10]. In this example, we have to detect the components of frequency of 20, 40 and 80 Hz. For this purpose, it is necessary to let $s1(n)$ go through a digital low-pass filter (cut-off frequency of pass band is at 40 Hz, cut-off frequency of stop band is at 50 Hz, ripple of pass band is 0.5 dB, attenuation of stop band is -45 dB). Consequently, we get a time series denoted by $s2(n)$ to detect $1/3X$ and $2/3X$. As for detecting $4/3X$, letting $s1(n)$ go through a high-pass filter (cut-off frequency of pass band is 75 Hz, cut-off frequency of stop band is 65 Hz, ripple of pass band is 0.5 dB, attenuation of stop band is -45 dB), we get another time series denoted by $s3(n)$. Therefore, we obtain a set of equations as follows:

$$\ddot{x} + 0.5\dot{x} - x + x^3 = 0.5 \times \hat{R}^1(\omega_1) \times \cos \omega_1 t + 0.1 \times s2(n),$$

$$\ddot{x} + 0.5\dot{x} - x + x^3 = 0.5 \times \hat{R}^1(\omega_2) \times \cos \omega_2 t + 0.1 \times s2(n),$$

$$\ddot{x} + 0.5\dot{x} - x + x^3 = 0.5 \times \hat{R}^1(\omega_3) \times \cos \omega_3 t + 0.1 \times s3(n),$$

where $\omega_1 = 2\pi \times 20$ rad, $\omega_2 = 2\pi \times 40$ rad, $\omega_3 = 2\pi \times 80$ rad. The corresponding bifurcation thresholds are $\hat{R}^1(125.664) = 1.655$, $\hat{R}^1(251.327) = 1.656$, $\hat{R}^1(502.655) = 1.689$, respectively. The solutions of this set of equations are shown in Figs. 7, 8 and 9, respectively. The corresponding maximum amplitudes of oscillators response are $A(\omega_1) = 1.719887$, $A(\omega_2) = 1.730571$, $A(\omega_3) = 1.752548$. According to Eq. (26), we can estimate the corresponding amplitudes of the exciting

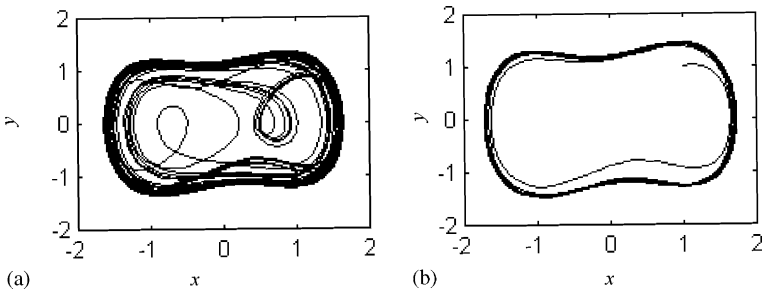

Fig. 7. Phase portraits without and with perturbation of $s2(n)$ (detecting $\omega = 2\pi \times 20$ rad): (a) no perturbation of $s2(n)$; (b) added perturbation of $s2(n)$.

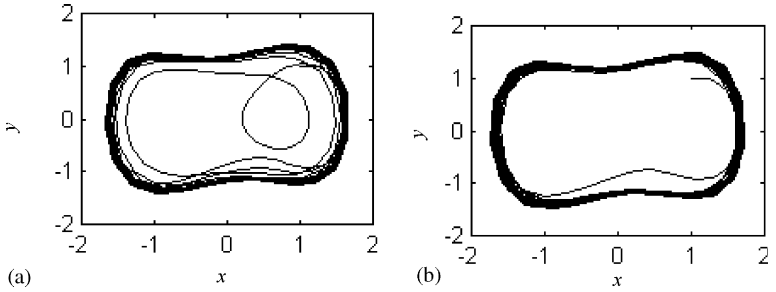

Fig. 8. Phase portraits without and with perturbation of $s2(n)$ (detecting $\omega = 2\pi \times 40$ rad): (a) no perturbation of $s2(n)$; (b) added perturbation of $s2(n)$.

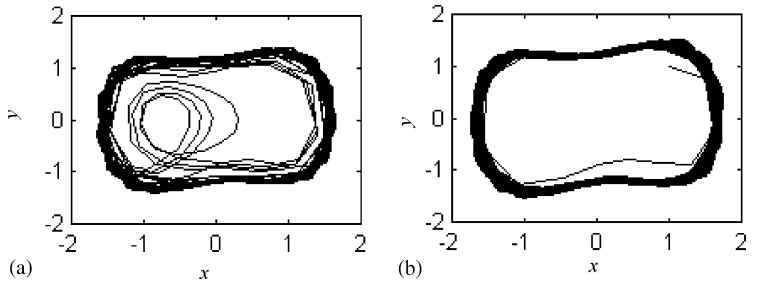

Fig. 9. Phase portraits without and with perturbation of $s3(n)$ (detecting $\omega = 2\pi \times 80$ rad): (a) no perturbation of $s3(n)$; (b) added perturbation of $s3(n)$.

signals:

$$a(\omega) = 0.2053, \quad \omega = 125.664,$$
$$a(\omega) = 0.3155, \quad \omega = 251.327,$$
$$a(\omega) = 0.3873, \quad \omega = 502.655.$$

6. Conclusion

This paper analyzes solutions and global bifurcations of Duffing equation and concludes that the large-scale periodic orbit furthest away from homoclinic orbits has the widest resonance band among solutions outside homoclinic orbits. The corresponding bifurcation threshold is obviously different from that of other orbits. The property of the threshold can be used to detect weak signal and suppress chaos. Furthermore, this paper gives an implementing model for detecting the weak signal based on Duffing oscillator and discusses related problems.

A detecting example presented in this paper demonstrates that the Duffing oscillator method for detecting the weak signal is very effective and reliable. One of the key points in machinery diagnostics is how to catch the symptoms of machine failure as early as possible. With this end in view, the chaotic oscillator model promises well for detecting the weak signal and for diagnosis of mechanical fault at early stage. However, it is necessary to do further research to determine

whether there are another chaotic oscillators suitable for detecting the weak signal in addition to Duffing oscillator.

Acknowledgements

The authors would like to acknowledge the support of National Natural Science Foundation of China (No. 59975025). The authors are grateful to Dr. Chen Min and Professor Pang Zhongming for their assistance in improving this paper. In particular, the authors would like to express their gratitude to Mr. Jim Tinsley, the foreign teacher of our university, for his aid in correcting this paper.

References

[1] L.B. Donald, Chaotic oscillators and CMFFNS for signal detection in noise environment, Proceedings of the IEEE International Joint Conference on Neural Networks, Baltimore, MD, Vol. 2, 1992, pp. 881–888.
[2] G.Y. Wang, D.J. Chen, J.Y. Lin, X. Chen, The application of chaotic oscillators to weak signal detection, IEEE Transactions on Industrial Electronics 46 (2) (1999) 440–444.
[3] W.L. Jiang, Y.Q. Wang, X.D. Kong, J.T. Li, New developments on hydraulic system fault detection and diagnostics, China Mechanical Engineering 9 (9) (1998) 58–62 (in Chinese).
[4] L.S. Qu, J. Lin, A difference resonator for detecting weak signals, Journal of Measurement 26 (1999) 69–77.
[5] B.D. Greenspan, P.J. Holmes, Homoclinic orbits, subharmonics, and global bifurcations in forced oscillators, in: G. Barenblaff, G. Iooss, D.D. Joseph (Eds.), Nonlinear Dynamics and Turbulence, Pitman, London, 1983, pp. 172–214.
[6] B.D. Greenspan, P.J. Holmes, Repeated resonance and homoclinic bifurcations in a periodically forced family of oscillators, SIAM Journal on Mathematical Analysis 15 (1984) 69–97.
[7] B.B. Okolewska, K. Czolczynski, T. Kapitaniak, J. Wojewoda, Chaotic Mechanics in Systems with Impacts and Friction, World Scientific, Singapore, 1999.
[8] M. Chen, N.Q. Hu, X.S. Wen, The application of chaotic oscillators in early detecting rub-impact fault of rotor system, Journal of National University of Defense Technology 23 (1) (2001) 36–39 (in Chinese).
[9] A. Muszynska, Partial lateral rotor to stator rubs, Proceedings of Third International Conference on Vibrations in Rotating Machinery, C281/84, ImechE, York, UK, 1984, pp. 327–335.
[10] N.Q. Hu, Y. Zhang, X.T. Hu, M. Chen, X.S. Wen, Experiment research on vibration characteristics of sharp rub-impact between rotor and stator, China Mechanical Engineering 13 (8) (2002) 777–779 (in Chinese).